applied sciences

MDPI

Article

Study of Cocoa Pod Husks Thermal Decomposition

Pablo Londoño-Larrea [1], Estefania Villamarin-Barriga [1], Angela N. García [2] and Antonio Marcilla [2,*]

[1] Chemical Engineering Faculty, Universidad Central del Ecuador, Ritter s/n & Bolivia, Quito 17-01-3972, Ecuador
[2] Department of Chemical Engineering, University of Alicante, P.O. Box 99, E-03080 Alicante, Spain
* Correspondence: antonio.marcilla@ua.es; Tel.: +34-965903867

Abstract: Thermal decomposition of cocoa pod husks under inert and oxidizing atmospheres was studied. Samples from Cotopaxi, Ecuador were used as raw material. Thermogravimetry based experiments were used to obtain decomposition data vs. temperature. A novel strategy to fit the TG and DTG curves was used giving good fit by considering, in the kinetic model, four biomass fractions following independent reactions. Analytical pyrolysis was used to determine the composition of volatile compounds obtained in slow (150–350, 350–500 °C) and flash pyrolysis (400 °C). The results indicate that in the slow pyrolysis experiments at low temperatures (150–350 °C), the highest area percentages correspond to ketones (7.5%), organic acids (12.5%) and phenolic derivatives (10%), while at increased temperatures (350–500 °C) the higher percentages are clearly focused on phenolic derivatives (12%) and aromatic compounds (10%). Comparing the results of flash pyrolysis at 400 °C (i.e., higher heating rate but lower final temperature), an increase in the yield of ketones and organic acids is observed compared to slow pyrolysis, but the percentage of phenols and aromatics decreases. The results obtained allow deducing the operating conditions to maximize the mass fraction of the different functional groups identified.

Keywords: pyrolysis; cocoa pod husks; volatile composition; kinetic analysis

Citation: Londoño-Larrea, P.; Villamarin-Barriga, E.; García, A.N.; Marcilla, A. Study of Cocoa Pod Husks Thermal Decomposition. *Appl. Sci.* **2022**, *12*, 9318. https://doi.org/10.3390/app12189318

Academic Editor: María Ángeles Martín-Lara

Received: 11 August 2022
Accepted: 12 September 2022
Published: 16 September 2022

1. Introduction

Ecuador is one of the biggest producers and exporters of cocoa, being the largest producer in America and ranking third worldwide. [1]. Locally, this industry generated 758 million of US dollars of income in 2021 due to the export of nearly 325,000 t of cocoa beans to forty different countries [2]. This implies a considerable amount of biomass residues generated during the process, mainly cocoa pod husk (CPH). These residues cannot be disposed of on the soil without any treatment because they may act as promoter to *Phytophthora* spp., the main cause of black pod rot [3]. Indeed, different studies have presented alternatives for using CPH residues such as anaerobic digestion [4], high value chemicals precursors [5–7], pectin extraction [8], and ash used as fertilizer [9,10], among others. Thus, for example, CPH was studied as a source of renewable energy through anaerobic digestion, where it has been possible to recover 54% of the chemical oxygen demand of the waste in the form of methane, being able to produce 8341 MWh annually. Although there are some published studies on the liquid fraction obtained from the thermal degradation of CPH, they are scarce. For example, liquid smoke from CPH pyrolysis at 147 °C was characterized using GC/MS, having methanol, acetic acid and acetol as main components [11]. In addition, the composition of biooil from CPH pyrolysis at 500 °C was studied using Zr-Fe based catalyst to obtain useful chemicals such as acetone, 2-butanone, phenol and alkyl phenols [12]. More studies have been reported that convert biomass into biochar via thermochemical treatment as a sustainable way to benefit from such residues, thus helping the environment by reducing greenhouse gases emissions, mainly atmospheric carbon as CO_2. Tsai et al. [13] obtained biochar from CPH under different conditions (190–370 °C and 30–120 min), evaluating its thermochemical properties and metal content.

Later, the same authors studied the surface area dependence on reaction temperature of CPH biochar obtained at 400–800 °C [14].

In other related studies, substantial improvements have been observed in the application of CPH biochar for greenhouse-scale cultivation of cocoa crops in Indonesia. The results of this study reported an improvement in the morphology of the plants compared to the control, specifically in: size of the plants, the number of leaves, area of the leaves and the root weight. However, the improvement in production could not be verified due to the time it takes for the crop to reach the reproductive phase [15]. Additionally, applications have been proposed for the complete utilization of the CPH by digestion combined with slow pyrolysis, to take advantage of all the pyrolysis products (gas, liquids and carbon). Under this scheme high quality biochars can be produced O/C = 0.06–0.10, H/C = 0.46–0.48, and up to 57.6% of the energy can be recovered [16].

In this work, the thermal decomposition of CPH has been studied from two points of view:

1. Thermogravimetric analysis, including the proposal of a kinetic model that allows adjusting the experimental data. In this line, a new fitting strategy is proposed. Although this strategy has been applied to the CPH decomposition, it can be extrapolated to any other TG/DTG experimental data.
2. Identification of the main volatiles obtained under different pyrolysis conditions, which can guide the selection of the best operating parameters to maximize a compound or a certain type of compounds.

The results presented here can be used as primary information for future applications of CPH.

2. Materials and Methods

2.1. Cocoa Pod Husk (CPH)

The CPH samples were obtained from a cocoa plantation in Moraspungo, Cotopaxi, Ecuador. The CPH was dried at 70 °C (simulating drying conditions in cocoa bean collection farms [17]) for 48 h at from 29.89% to 10.47% humidity, and then milled to a mesh size of 1 cm using the cutting mill Retsch SM300. The samples were mixed and homogenized prior to all test procedures.

2.2. Thermogravimetric Analysis (TGA)

TGA was used to perform a proximal analysis of CPH in a single experiment, based on previous works [18,19], achieving similar results to those obtained by ASTM methods. TGA runs were carried out using Mettler-Toledo TGA1 equipment, starting at 25 °C with a N_2 atmosphere (20 mL min^{-1}) and increasing the temperature to 100 °C at 10 °C min^{-1} during 15 min (moisture determination). Afterwards, temperature was increased up to 700 °C at 10 °C min^{-1} (volatile matter and fixed carbon determination). Then, the atmosphere was changed from nitrogen to air, 50 mL min^{-1}, hold time 30 min (ash determination). The run was carried out at 540 mmHg (atmospheric pressure in Quito).

DTG was used as an approximation to obtain the percentages of hemicellulose (HC), cellulose (CL) and lignin (LG) containing the volatile fraction, using deconvolution of characteristic peaks formed. This method is faster, easier to implement and less expensive than traditional methodologies. Working with lignocellulosic samples it has been concluded that this approach leads to cellulose and hemicellulose percentages comparable with those obtained with chemical methods. In the case of lignin determination, the deconvolution method is less accurate due to the wide range of temperatures in which it decomposes [19].

Additionally, experiments at different heating rates (5–20 °C min^{-1}) were carried out under inert and oxidative atmospheres to perform a kinetic analysis, from 25 to 700 °C, 50 mL min^{-1} gas flow.

2.3. Elemental Analysis

Elemental analysis was carried out on Elementar Vario Macro Cube. Oxidation and reduction temperatures were established at 1150 °C and 850 °C, respectively. Two blank samples were used to establish baseline with oxygen and without oxygen, and three standard samples were analyzed to adjust the equipment daily values (k-factor) using sulfanilamide as the test standard. Approximately 10 mg of sample was used for analysis and 0.1 mg of tungsten oxide as oxidation catalyst. The percentage of N, C, S and H obtained from the equipment was directly recorded for each sample. The percentage of oxygen was obtained by difference using the ash value obtained by thermogravimetry.

2.4. Analytical Pyrolysis EGA Analysis

This technique consists of reacting the sample in an oven located just above the GC-MS injection port, concentrating the gases produced and injecting them directly into the GC. An Agilent model 7820B chromatograph coupled to an Agilent model 5977B mass spectrometer was used.

The method was set as follows: HP-5 ms Ultra Inert column (30 m × 250 µm × 0.25 µm) was used to separate the molecules with He as carrier gas at 2 mL min^{-1}. The reaction oven was purged with N_2 and heated to the desired temperature for each experiment. The gases from the pyrolysis were injected in split mode (50:1) at a temperature of 280 °C. The oven program started at 45 °C for 5 min and increased to 285 °C at 12 °C min^{-1}, keeping the final temperature constant for 10 min. The transfer line temperature was set at 300 °C. The MS source was set at 230 °C and the quadrupole at 150 °C. The detection type was set at scan mode with an initial mass 15 and a final mass 350. This method is similar to those reported before [20]. Two types of experiments were performed:

- Flash pyrolysis at 400 °C
- Slow pyrolysis at three different temperature ranges: 80–150 °C, 150–350 °C and 350–500 °C. The heating rate was 50 °C min^{-1}.

3. Results and Discussion

3.1. CPH Characterization

CPH was characterized in terms of proximate, elemental and physicochemical analysis (Table 1). Previous studies on the characterization of cocoa shells have obtained similar results to those of this work. For example, Vriesmann et al. [8] obtained values for 8.5% for humidity and 6.7% for ash in CPH samples obtained in Brazil. Fei Lu et al. [21] have reported ash between 6.4 and 8.4% for cocoa husks from Ghana. Likewise, Ghysels et al. [16] carried out the complete characterization of the cocoa shell from the province of Manabí-Ecuador, obtaining the following proximal composition: 3.8% humidity, 67.13% volatile material, 11.38% ashes, 21.49% fixed carbon. From the elemental analysis they obtained the following values: 43.55% C, 5.18% H, 38.51% O. In addition, determining the pH (1 g of sample in 20 mL of deionized water, 1.5 h stirring [22]) at 5.52 and the calorific value at 16.49 MJ kg^{-1}.

Table 1. Physicochemical characterization of cocoa pod husk (CPH).

Variable	Unit	Value
Initial moisture	%	29.9 ± 6.3
Final moisture	%	10.5 ± 0.2
Volatile matter	%	59.4 ± 1.2
Fixed carbon	%	21.4 ± 0.4
Ash	%	8.8 ± 0.2
Surface area	$m^2\ g^{-1}$	0.24 ± 0.01
C	%	41.5 ± 1.0
N	%	1.69 ± 0.11

Table 1. *Cont.*

Variable	Unit	Value
H	%	6.2 ± 0.2
O *	%	41.6 ± 1.0
S	%	0.20 ± 0.04
Empiric formula	-	$CH_{1.79}N_{0.03}O_{0.75}$
H/C molar ratio		1.79 ± 0.07
O/C molar ratio		0.75 ± 0.03
HHV **	MJ kg^{-1}	17.3 ± 0.4
Hemicellulose ***	%	21.2 ± 0.4
Cellulose ***	%	23.2 ± 0.5
Lignin ***	%	15.0 ± 0.3
pH	-	5.7 ± 0.1
Electrical conductivity	mS	6.7 ± 0.2

* Obtained by difference; ** Higher heating value obtained from elemental analysis and Gaur—Reed equation [23]; *** Approximation obtained from deconvolution of DTG.

3.2. Thermal Decomposition of CPH

The study of the thermal decomposition of CPH was carried out using the TGA and the method described previously. Figure 1 shows the TG and DTG curves obtained using different atmospheres and heating rates.

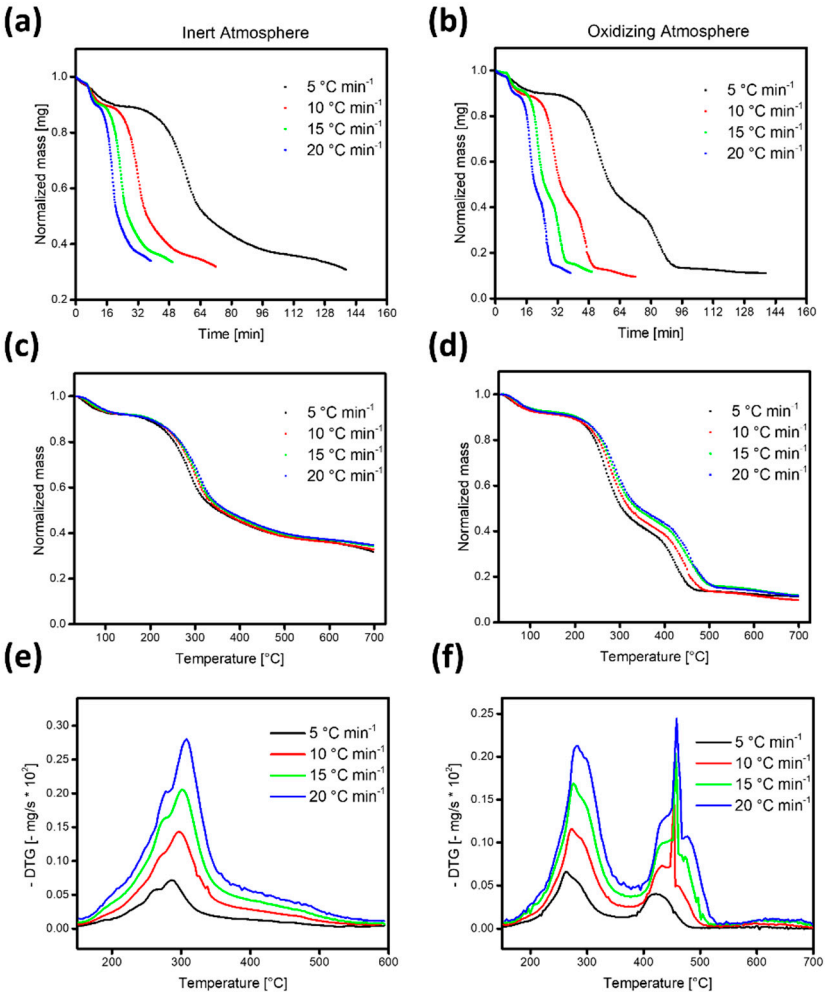

Figure 1. Thermal decomposition of cocoa shells in TG using different atmospheres and heating rates. (**a**,**c**) inert atmosphere; (**b**,**d**) oxidizing atmosphere. DTG curves (**e**) inert atmosphere; (**f**) oxidizing atmosphere.

The mass loss curves as a function of time (Figure 1a,b) shift to the left (lower times) by increasing the heating rate and, as was expected, the opposite behavior is observed in the mass loss curves as a function of temperature (Figure 1c,d), that shift slightly to the right (higher temperatures). Although this displacement is not very large, it is noticeable, especially under air atmosphere. This type of behavior has been previously observed in other biomass kinetic studies and has been mathematically interpreted using kinetic equations [24–26]. Thus, it has been shown that only considering the kinetics of the process, without taking into account possible changes in mechanisms or poor heat transfer, the position of the maximum peak of DTG can be expressed as a function of the heating rate [27,28], so that with a higher heating rate, the maximum peak is located at a higher temperature. Physically, it can be visualized by considering that at low heating rates the sample remains for longer times at each temperature interval, and consequently it has more chances for reacting; the peaks thus appear at lower temperatures as compared with higher heating rates. Furthermore, the magnitude of this displacement depends on the kinetic parameters of the process: the higher the activation energy and the lower the pre-exponential factor, the greater the displacement magnitude [29].

The differences between the curves obtained in an inert atmosphere (Figure 1e) and an oxidizing atmosphere (Figure 1f) are seen around 400 °C, where the oxidation and combustion reactions of the biomass begin, giving rise to a greater weight loss. In the case of the oxidizing atmosphere, two decomposition zones are clearly distinguished, one more centred around 280 °C (more related to pyrolysis) and the other around 450 °C (more related to combustion). A sharp peak around 480 °C is also observed, influenced by the heating rate (it does not appear at 5 °C min^{-1}) and which has already been observed in the decomposition of other biomasses in an oxidizing atmosphere. This peak would correspond to the reaction of the fraction of the carbonaceous residue that is being formed in the decomposition process and that is more accessible to oxygen (for example char arranged in cracks, as superficial sheets or as fine particles) and that reacts very quickly, while the rest of the residue reacts more gradually. A fourth reaction (appreciable above 600 °C) can be related to the decomposition and reaction of the inorganic fraction of the biomass. As expected, different values of the final weight were obtained in each reaction atmosphere, since in an oxidizing atmosphere the combustion of fixed carbon occurs, leaving only the ashes as residue.

3.3. Kinetic Model and Fitting Strategy

During the thermal decomposition of biomass, different regions of weight loss can be observed. Each region is considered a fraction that turns into volatile material and solid residue (except for the region identified as moisture). Combustion of solid material gives rise to ashes.

In the literature, different kinetic models have been proposed that allow adjusting the thermal decomposition curves of different biomasses. However, only those models that describe thermal decomposition at different heating rates using the same kinetic constants are considered valuable. Here, a model of independent decomposition reactions has been considered, each one corresponding to a fraction of the biomass that decomposes in a different temperature range. In short, the model can be represented as:

$$w_{i_0} W_i \rightarrow (w_{i_o} - v_{i_\infty}) C_i + v_{i_\infty} V_i \quad (1)$$

where W_i corresponds to each one of the original biomass fractions, V_i corresponds to the volatiles released during its decomposition, C_i is the carbonaceous residue formed as a product of the reaction, $v_{i\infty}$ corresponds to the maximum mass fraction of the volatiles and w_{io} is the initial mass fraction of each fraction. Considering m as the number of different fractions that make up the biomass, the following can be expressed:

$$\sum_{i=1}^{m} w_{i_0} = 1 \quad (2)$$

The experimental data have been normalized to zero residue which, for practical purposes of the model, would be equivalent to considering $v_{i\infty} = w_{i_0}$. When considering kinetics of order n, the thermal decomposition equation of each one of the biomass fractions can be represented as:

$$-\frac{dw_i}{dt} = k_i {w_i}^{n_i} \tag{3}$$

where w_i is the mass fraction of W_i at each moment, k_i is the kinetic constant of the decomposition reaction and n_i is the reaction order. Considering that k_i can be expressed using the Arrhenius equation

$$k_i = k_{0_i}\, exp\left(-\frac{E_i}{RT}\right) \tag{4}$$

the equation that describes the kinetics of m components is expressed as:

$$-\frac{dw_i}{dt} = k_{0_i}\, exp\left(-\frac{E_i}{RT}\right) {w_i}^{n_i} \text{ where } i = 1, 2, 3, \ldots, m \tag{5}$$

The most common strategy to solve this equation, finding values for k_{0_i}, E_i and n_i that describe the kinetics of m components, consists in the successive iteration minimizing the error between the experimental value and the calculated one, using tools such as "Solver" of Microsoft Excel® (Microsoft Excel 2019 MSO (16.0.10389.20033), Microsoft Corporation, Redmon, WA, USA), or similar. Using a reference temperature to minimize the interrelation among the kinetic parameters is widely used [30].

A more powerful strategy would consist of obtaining the second derivative of the kinetic equation and setting it equal to zero, in order to obtain the mathematical expression that defines the maximum of the absolute value of the weight derivative with respect to time, thus:

$$-\frac{d^2 w_i}{dt^2} = k_{0_i}\, exp\left(-\frac{E_i}{RT}\right) {w_i}^{n_i} \left[\left(\frac{E_i}{R}\right)\frac{\beta}{T^2} - k_{0_i} exp\left(-\frac{E_i}{RT}\right) n_i {w_i}^{n_i - 1}\right] = 0 \tag{6}$$

$$\frac{E_i\, w_i \beta}{RT^2} - n_i\, k_{0_i}\, exp\left(-\frac{E_i}{RT}\right) {w_i}^{n_i} = 0 \tag{7}$$

This expression introduces the known variable β (heating rate) into the equation and allows establishing the temperature range in which the maximum for each component is visually identified, restricting the solution of each temperature to its respective range, and thus obtaining an improved convergence. From Equation (7), the expression used for k_{0_i} calculation can be deduced:

$$k_{0_i} = \beta \frac{E_i}{R} {w_i}^{1-n_i}\, exp\left(\frac{E_i}{RT}\right) T^{-2} {n_i}^{-1} \tag{8}$$

Additionally, it has been considered to give a flexibility window of up to ±5 °C for each T obtained experimentally, so that the optimization process better adjusts each heating rate, considering this temperature dispersion that can be common in this type of experiments. In Equation (8), the value w_i = 0.5 has been set as an arbitrary value (note that the maximum weight loss rate is close to the temperature where the remaining weight fraction is 0.5) to run the model and find the values of T, k_{0_i}, E_i and n_i that minimize the error between the calculated and the experimental curves (objective-error function) of TG and DTG, calculated as follows:

$$OF = \sum_j \sum_i \left[\left(w_{exp_{ij}} - w_{calc_{ij}}\right)^2 + 2{\cdot}10^4 \left(\left(\frac{dw}{dt}\right)_{exp_{i,j}} - \left(\frac{dw}{dt}\right)_{calc_{i,j}}\right)^2\right] \tag{9}$$

with i being the data obtained for each time t and j the data obtained for each heating rate β. The difference between calculated and experimental DTG values has been multiplied by a factor to balance the weight of TG and DTG in the objective function.

In order to take into account the number of points in each adjustment as well as the number of parameters used and the mean value of the experimental points considered in the fitting ($P_{average}$), a variation coefficient (VC) has been calculated according to the following expression:

$$VC(\%) = \frac{\sqrt{\frac{OF}{n\ points - n\ parameters}}}{P_{average}} \cdot 100 \quad (10)$$

The value of $P_{average}$ has been considered as 0.5, since the TG curves were normalized with the values moving from 1 to near 0, and values of DTG had been multiplied by 20,000 in the objective function to balance the weight of TG and DTG.

3.4. Kinetic Parameters

The kinetic study of thermal decomposition of CPH was carried out in different reaction atmospheres and heating rates of 5, 10, 15 and 20 °C min^{-1}. First, the adjustment was made individually for each heating rate in a nitrogen atmosphere. Using this strategy, a very good fit was obtained for each experiment (Figure 2) and VC values are in the range 0.5–1.6%.

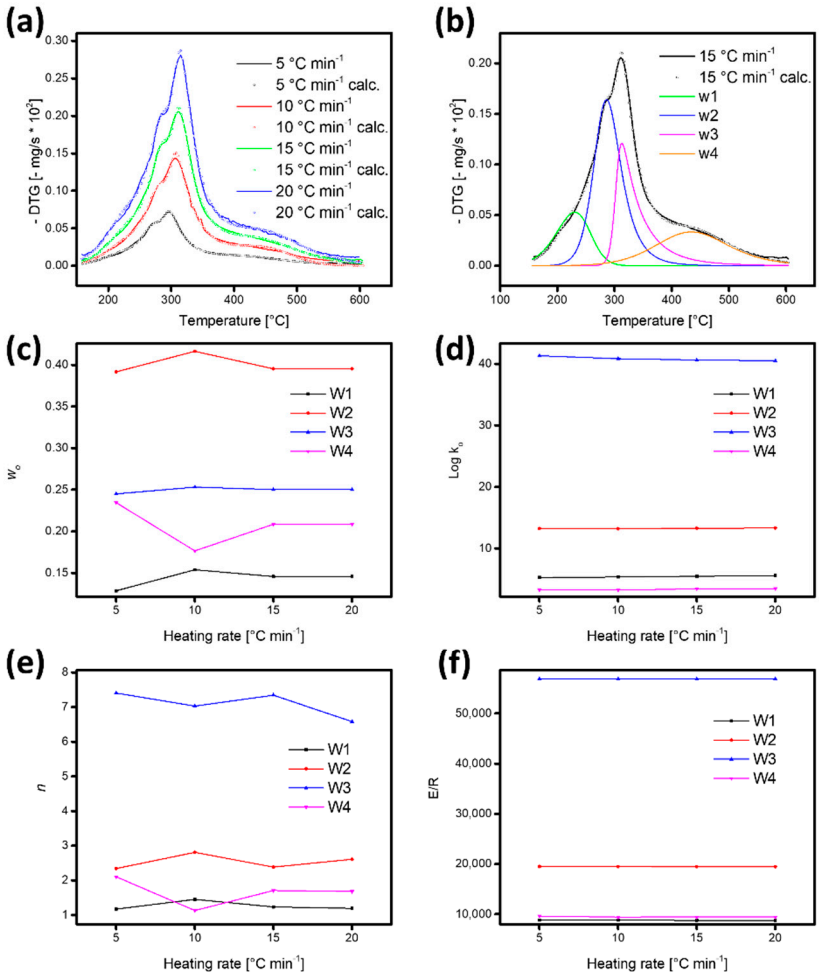

Figure 2. Individual fit of CPH thermal decomposition experiments in inert atmosphere for each heating rate. (**a**) comparison of experimental and calculated data, (**b**) example of the four fractions obtained in the fitting at 15 °C min^{-1}, (**c**) variation of the w_o values, (**d**) variation of the $log\ k_o$ values, (**e**) variation of the n values, (**f**) variation of the E/R values.

As can be seen in Figure 2a, the kinetics fit is very good for all heating rates. The adjustment was achieved considering four biomass decomposition fractions, i.e., 4 independent reactions. According to the temperature ranges where the decomposition processes take place (Figure 2b), fractions 2, 3 and 4 are related to hemicellulose, cellulose and lignin, respectively, and fraction 1 is related to lighter extractives present in CPH, such as pectine. Furthermore, these fractions can also include the residues generated in the decomposition processes of hemicellulose, cellulose, lignin and extractives and that decompose more slowly. The variation of each kinetic parameter for each component as a function of the heating rate can be visualized in Figure 2c–f. The values shown, despite having been obtained from individual fittings, did not present a significant variation with the heating rate.

With this background, the model proposed has been used to fit simultaneously the TG and DTG curves obtained at the 4 heating rates, reaching the kinetic parameters representative of the thermal decomposition of CPH under inert atmosphere. Figure 3 compares experimental and calculated curves and Table 2 shows the kinetic parameters obtained. In this case, the VC value is 2.7%.

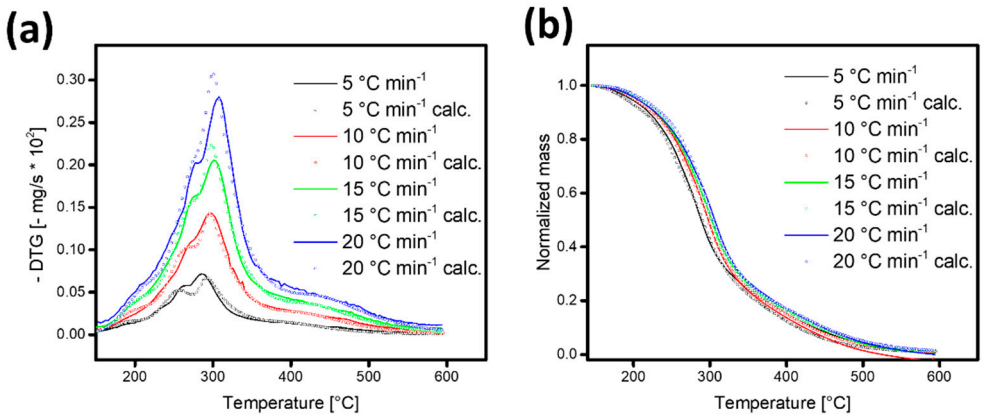

Figure 3. Fit of CPH thermal decomposition experiments under inert atmosphere. (**a**) DTG, (**b**) TG.

Table 2. Kinetic parameters of CPH thermal decomposition experiments at inert atmosphere. Overall adjustments of the four heating rates.

Parameter	W_1	W_2	W_3	W_4
k_0 (s^{-1})	1.87×10^9	2.74×10^{13}	1.41×10^{40}	1.20×10^7
E/R	12,527.41	19,130.53	54,889.86	15,032.63
E ($kJmol^{-1}$)	104.16	159.06	456.38	124.99
n	4.20	2.80	8.40	2.64
w_0	0.18	0.37	0.32	0.14

The adjustment in this case is less precise than the one obtained for each heating rate independently. This was expected due to the complexity of the overlapping decomposition processes and the increasing number of data fitted simultaneously. However, despite the above, the results obtained in the overall fit are good and the values of the kinetic parameters are similar to others previously obtained in biomass kinetic studies. Hameed et al. [31] summarize the information from several articles on biomass pyrolysis kinetics, where values of activation energy (E) from 36 to 192 kJ mol^{-1} and frequency factor (k_0) up to 1.7×10^{21} s^{-1} are found.

The same treatment was performed for the data obtained under oxidizing atmosphere and the results can be seen in Figure 4 and in Table 3. Similarly to the case of inert atmosphere, the VC value is 2.7%.

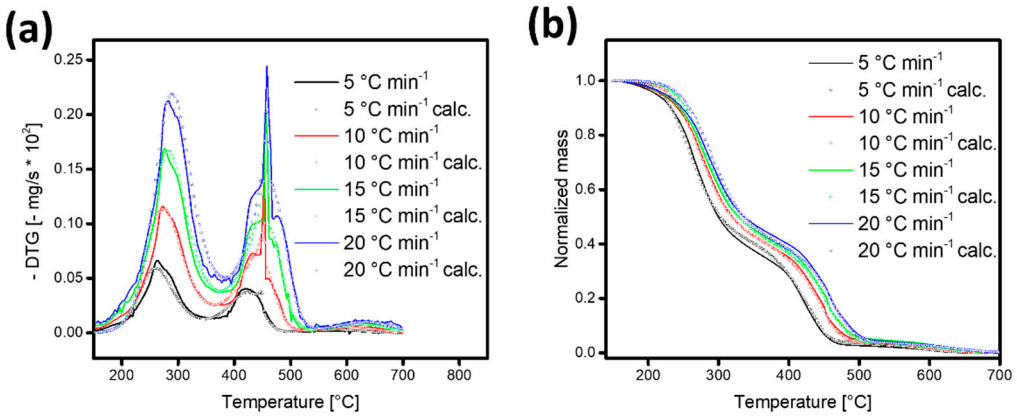

Figure 4. Fit of CPH thermal decomposition experiments in oxidizing atmosphere. (**a**) DTG, (**b**) TG.

Table 3. Kinetic parameters of CPH thermal decomposition experiments in oxidizing atmosphere. Overall adjustments of the four heating rates.

Parameter	W_1	W_2	W_3	W_4
k_0 (s^{-1})	2.95×10^8	3.29×10^7	4.77×10^{49}	9.39×10^6
E/R	13,333.08	16,066.52	85,362.67	18,950.29
E ($kJmol^{-1}$)	110.86	133.58	709.75	157.56
n	2.49	1.13	0.65	1.37
w_0	0.61	0.33	0.02	0.04

In the case of the oxidizing atmosphere, two decomposition zones are clearly distinguished, one more centered at around 280 °C and the other around 450 °C. According to these results, the behavior of the curves can be explained by considering four different processes: two main reactions, one more related to pyrolysis and the other to combustion; a third reaction corresponding to some fraction of the initial biomass or coming from the char itself that is being formed and that reacts more violently than the rest, may be a superficial char or more labile char in cracks, at high heating rates (sharp peak around 480 °C). A fourth reaction (appreciable above 600 °C) may come from the decomposition and reaction of the inorganic fraction of the biomass.

3.5. Analytical Pyrolysis EGA Analysis

A series of experiments were carried out in EGA in order to determine the composition of volatiles generated under different conditions. On the one hand, a slow pyrolysis of CPH was carried out, determining the volatiles distribution at three different temperature ranges: 80–150 °C, 150–350 °C and 350–500 °C. On the other, flash pyrolysis at 400 °C was also performed, determining the composition of the volatiles obtained.

As was expected, the presence of aromatics, phenol derivatives, furan and pyran derivatives, ketones, carboxylic acids as well as nitrogen compounds is detected in the volatiles obtained, but their percentage and distribution depend on the operating conditions, such as final temperature and heating rate.

By analyzing the results of the slow pyrolysis, it is observed that the product distribution obtained is very different in the 3 ranges analyzed:

1. 80–150 °C. Only water is detected in this range. The temperature is not high enough to release any other volatiles.
2. 150–350 °C. Besides water and CO_2, which are the main compounds detected, 3 other compounds clearly stand out among all: acetic acid, 2,6-dimethoxy-4-(2-propenyl)-phenol and 1-hydroxy-2-propanone. The presence of other ketones, phenol derivatives and organic acids is detected in lower percentages.
3. 350–500 °C. By increasing temperature, the number of volatiles formed increases. In fact, the total chromatographic area obtained in this range is 20% higher than the area

obtained in the previous one. Water and CO_2 continue to be the main compounds, but a greater number of volatiles, more than 200, is detected. The yields of all of them are more similar and, unlike the previous temperature range, the compounds with higher percentages do not stand out too much from the rest. The increase in temperature has increased the generation of compounds but has decreased the selectivity of the process, i.e., many more compounds with lower yield. The 3 compounds with the highest area percentage are 2-methoxy-phenol, toluene and 2-methyl-furan. Many other phenol derivatives (4-methyl-phenol, 2,3-dimethyl-phenol, 2-methoxy-4-propyl-phenol, 2,6-dimethoxy-4-(2-propenyl)-phenol), aromatics (benzene, ethylbenzene, xylene, naphthalene derivatives), organic acids (C16, C18) and other functional groups are also identified.

The differences in the type of compounds obtained from one temperature range to another reveal the fraction of the biomass which is decomposing in each interval. Thus, between 150–350 °C, hemicellulose has been totally degraded, generating the highest yields of acetic acid [32,33]. However, phenol derivatives and other aromatics show their maximum percentage at higher temperatures, in the range 350–500 °C, when the lignin fraction has reached a high degradation level [32,34].

Table 4 shows the area percentage of the volatiles identified with a percentage greater than 1%, for both temperature ranges. The values have been calculated with respect to the total area excluding CO_2, i.e., the area related to condensable volatiles, except for the value of this compound which has been referred to the total area.

Table 4. Area percentage of main compounds.

T process (°C)	Compound	% Area *
150–350	CO_2	17
	water	22
	acetic acid	8.3
	2-propanone,1-hydroxy-	3.3
	2-cyclopenten-1-one, 2-hydroxy-	1.4
	phenol,2-methoxy-4-(1-propenyl)-	1.8
	phenol,2,6-di-methoxy-4-(2-propenyl)-	4.9
	hexadecanoic acid	1.6
	9-octadecenoic acid	1.3
	octadecanoic acid	1.2
350–500	CO_2	9.4
	water	12
	furan, 2-methyl	1.0
	toluene	1.4
	phenol,2-methoxy	1.6
400 (flash)	CO_2	22
	acetic acid	6.5
	2-propanone,1-hydroxy-	4.3
	2-cyclopenten-1-one + furfural	1.1
	2-cyclopenten-1-one, 2-hydroxy-	1.3
	2-methoxy-4-vinylphenol	1.0
	phenol,2-methoxy-4-(1-propenyl)-	1.0
	phenol,2,6-di-methoxy-4-(2-propenyl)-	1.0
	hexadecanoic acid	3.2
	9-octadecenoic acid	1.9
	octadecanoic acid	1.7

* Area percentage calculated with respect to (total area—CO_2 area), except CO_2 which has been referred to the total area.

The results obtained in the flash pyrolysis of CPH at 400 °C showed an intermediate behavior between the temperature ranges of the slow pyrolysis described previously. Around 70 compounds have been detected, of which CO_2 (mainly), acetic acid, 1-hydroxy-

2-propanone and n-hexadecanoic acid stand out from the rest. No water has been identified in this process. A high number of cyclopentanone derivatives (2-cyclopenten-1-one, 2-cyclopenten-1-one, 2-hydroxy-, 2-cyclopenten-1-one,2-methyl-, 2-cyclopenten-1-one,2-hydroxy-3-methyl-, 3,5-dimethyl-cyclopentane-1,2-dione among others) coming from cellulose pyrolysis [35] is observed, while the number of phenolic derivatives obtained is much lower than that detected in slow pyrolysis up to 500 °C. Among the compounds of this group, it is worth highlighting phenol,2,6-di-methoxy-4-(2-propenyl)-, phenol,2-methoxy-4-(1-propenyl)- and 2-methoxy-4-vinylphenol, with the highest area percentages. Table 4 includes the compounds obtained with an area percentage greater than 1%.

Besides the area percentage of the main compounds identified (Table 4), it is also interesting to compare the area/mg sample values for these compounds in the experiments carried out, since these values are representative of the product yields obtained in each case.

Figure 5 compares the area/mg sample of different compounds obtained in the 3 types of experiments. The addition of the results corresponding to 150–350 °C and 350–500 °C has been also included in the figure, in order to have a better comparison with the flash pyrolysis result.

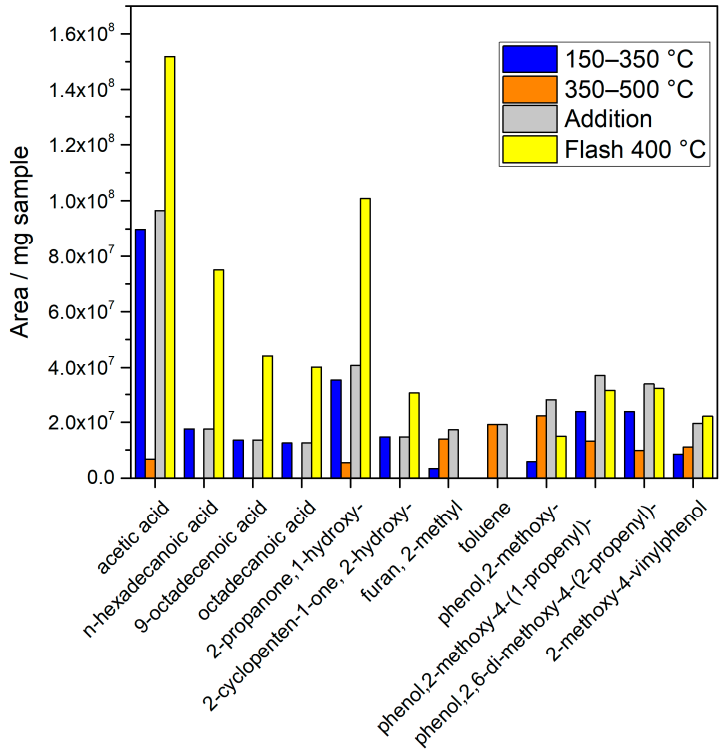

Figure 5. Comparison of area/mg sample values of different pyrolytic compounds under different conditions.

In Figure 5, it can be seen how flash pyrolysis at 400 °C significantly increases the yield of some compounds compared to pyrolysis at higher temperature (up to 500 °C when considering the sum of the 2 slow pyrolysis intervals) but lower heating rate. These compounds are organic acids and ketones, that is, compounds that come mainly from the thermal decomposition of hemicellulose and cellulose. They are compounds that in the slow pyrolysis at 350 °C had already been generated fairly completely and an additional pyrolysis up to 500 °C does not increase their yield significantly. However, an increase in heating rate does. Other compounds, such as furan,2-methyl and toluene, which had hardly formed in the 150–350 °C range, were also not detected in flash pyrolysis at 400 °C. In the case of the main phenolic derivatives, coming from the decomposition of lignin, the increase in the heating rate cannot improve the yield obtained in slow pyrolysis, but the yields achieved in flash pyrolysis at 400 °C have been very similar to those of slow pyrolysis up to 500 °C.

In order to improve the analysis of the results, all the compounds identified were grouped according to their main functional group: ketones + aldehydes (KA), organic acids + esters (OAE), furan/pyran derivatives (FP), nitrogen compounds (NC), phenol derivatives (PD), aromatics (AR) and hydrocarbons (HC).

Figure 6 shows the comparison of the percentages obtained for each group in the temperature ranges studied and Figure 7 shows a similar comparison for the area/mg sample values.

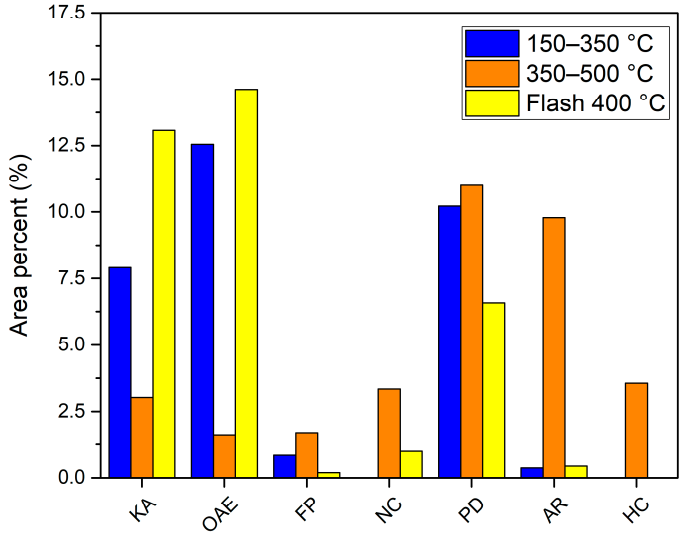

Figure 6. Comparison of area percentages for the different functional groups.

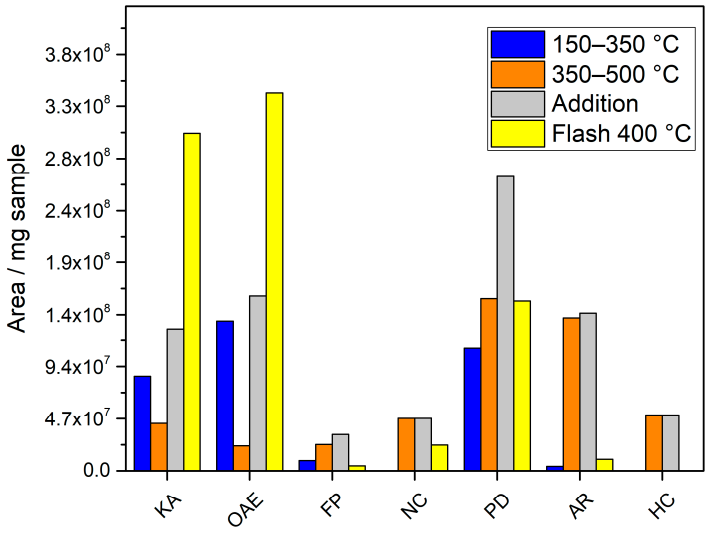

Figure 7. Comparison of area/mg sample values for the different functional groups.

If it is considered that the area percentage of a compound can be representative of its mass fraction in the bio-oil obtained, Figure 6 will allow deducing the operating conditions to maximize the mass fraction of the different functional groups identified. Thus, it is observed that if the bio-oil fraction generated in a slow pyrolysis between 350–500 °C is selected, a liquid fraction rich in phenolic and aromatic derivatives, with a lower percentage of other type of compounds, will be obtained. In contrast, it is interesting to pyrolyze at intermediate temperatures (350–400 °C), to maximize the fraction of ketones and organic acids.

Figure 7 allows estimating not mass fractions, but global yields. This figure shows a clear difference between slow and flash pyrolysis to obtain ketones and organic acids,

in favor of the latter. In the rest of the functional groups, and especially in the case of phenolic and other aromatic derivatives, it seems that, in the range of values studied, a greater increase in yield is achieved with an increase in temperature, rather than with an increase in the heating rate.

4. Conclusions

Thermochemical decomposition of cocoa pod husk (CPH) was studied under inert and oxidizing atmospheres. The TG and DTG curves fit satisfactorily considering that the original sample is formed by 4 fractions that decompose following independent reactions. According to the decomposition temperature ranges of each of these components, they are related to the fractions of extractives, hemicellulose, cellulose and lignin of the CPH, as well as the residues that are generated during the decomposition process and that continue to decompose until the final char.

A new fitting strategy has been proposed consisting of calculating the second derivative of the kinetic equation and setting it equal to 0, in order to obtain the mathematical expression that defines the maximum of the absolute value of the weight derivative. This fact improves the convergence of the fit.

A different spectrum of the pyrolytic volatiles is obtained as a function of the temperature and the heating rate of the process. The main area percentages are reached for acetic acid (8.3%), 2-propanone, 1-hydroxy (3.3%) and phenol,2,6-di-methoxy-4-(2-propenyl)- (4.9%) in slow pyrolysis (150–350 °C) and for acetic acid (6.5%), 2-propanone, 1-hydroxy (4.3%) and hexadecanoic acid (3.2%) in flash pyrolysis at 400 °C. Slow pyrolysis in the range 350–500 °C significantly increases the number of compounds detected (mainly phenolic and aromatic derivatives) but reduces the area percentages (<1.6%).

When comparing the yields of the compounds obtained in slow pyrolysis up to 500 °C and flash pyrolysis at 400 °C, it is observed that by increasing the heating rate (flash pyrolysis) increases the yield of ketones and organic acids (area/mg sample) by 2.5–3 times. In the case of the yield of aromatic compounds and phenolic derivatives, the increase in the heating rate has not been able to counteract the decrease in temperature, and flash pyrolysis at 400 °C has significantly reduced the generation of these compounds. Therefore, according to the results obtained, yields of ketones and organic acids are highly affected by the heating rate, showing significant differences between slow and flash pyrolysis, while phenolic and other aromatic derivatives are more affected by the pyrolysis temperature in the range of values studied.

Author Contributions: Conceptualization, formal analysis and project administration A.M. and A.N.G.; methodology and analysis P.L.-L. and E.V.-B. All authors contributed to reviewing and writing. All authors have read and agreed to the published version of the manuscript.

Funding: This research was funded by "Conselleria d'Educació, Investigació, Cultura i Esport" (ID-IFEDER 2018/009), "Universidad Central del Ecuador" (International Collaboration Agreement Nº 061-P-05) and "Universidad de Alicante" (UA grant 'Development Cooperation' BOUA 5/05/2021).

Institutional Review Board Statement: Not applicable.

Informed Consent Statement: Not applicable.

Data Availability Statement: Not applicable.

Conflicts of Interest: The authors declare no conflict of interest. The funders had no role in the design of the study; in the collection, analyses, or interpretation of data; in the writing of the manuscript; or in the decision to publish the results.

References

1. Shahbandeh, M. Cocoa Bean Production Worldwide 2018/19 & 2020/21, by Country. Available online: https://www.statista.com/statistics/263855/cocoa-bean-production-worldwide-by-region/ (accessed on 28 August 2022).
2. Agencia de Regulación y Control Fito y Zoosanitario Cocoa Export during 2021. Available online: https://www.agrocalidad.gob.ec/wp-content/uploads/2022/02/Informe-cacao.pdf (accessed on 28 August 2022).

3. Acebo-Guerrero, Y.; Hernández-Rodríguez, A.; Heydrich-Pérez, M.; El Jaziri, M.; Hernández-Lauzardo, A.N. Management of Black Pod Rot in Cacao (*Theobroma Cacao* L.): A Review. *Fruits* **2012**, *67*, 41–48. [CrossRef]
4. Acosta, N.; De Vrieze, J.; Sandoval, V.; Sinche, D.; Wierinck, I.; Rabaey, K. Cocoa Residues as Viable Biomass for Renewable Energy Production through Anaerobic Digestion. *Bioresour. Technol.* **2018**, *265*, 568–572. [CrossRef] [PubMed]
5. Golveia, J.C.S.; Bara, M.T.F.; Santiago, M.F.; Campos, L.C.; Schimidt, F. Cocoa Agro-Industrial Residue (*Theobroma cacao*) as Inducer of the Production of Fungal Laccase and Kojic Acid for Application in the Biodegradation of 17-α-Ethinylestradiol. *J. Braz. Chem. Soc.* **2020**, *31*, 2023–2029. [CrossRef]
6. Yusof, F.; Khanahmadi, S.; Amid, A.; Mahmod, S.S. Cocoa Pod Husk, a New Source of Hydrolase Enzymes for Preparation of Cross-Linked Enzyme Aggregate. *Springerplus* **2016**, *5*, 57. [CrossRef] [PubMed]
7. Campos-Vega, R.; Nieto-Figueroa, K.H.; Oomah, B.D. Cocoa (*Theobroma cacao* L.) Pod Husk: Renewable Source of Bioactive Compounds. *Trends Food Sci. Technol.* **2018**, *81*, 172–184. [CrossRef]
8. Vriesmann, L.C.; de Mello Castanho Amboni, R.D.; de Oliveira Petkowicz, C.L. Cacao Pod Husks (*Theobroma cacao* L.): Composition and Hot-Water-Soluble Pectins. *Ind. Crops Prod.* **2011**, *34*, 1173–1181. [CrossRef]
9. Ayeni, L.S. Integrated Application of Cocoa Pod Ash and NPK Fertilizer on Soil Chemical Properties and Yield of Tomato. *Am. J. Sustain. Agric.* **2008**, *2*, 333–337.
10. Ayeni, L.S.; Adetunji, M.T.; Ojeniyi, S.O.; Ewulo, B.S.; Adeyemo, A.J. Comparative and Cumulative Effect of Cocoa Pod Husk Ash and Poultry Manure on Soil and Maize Nutrient Contents and Yield. *Am. J. Sustain. Agric.* **2008**, *2*, 92–97.
11. Putri, R.E.; Kasim, A.; Emriadi; Asben, A. Pyrolysis and Characterization of Liquid Smoke from Cacao Pod Husks. *IOP Conf. Ser. Earth Environ. Sci.* **2019**, *327*, 012011. [CrossRef]
12. Mansur, D.; Tago, T.; Masuda, T.; Abimanyu, H. Conversion of Cacao Pod Husks by Pyrolysis and Catalytic Reaction to Produce Useful Chemicals. *Biomass Bioenergy* **2014**, *66*, 275–285. [CrossRef]
13. Tsai, C.-H.; Tsai, W.-T.; Liu, S.-C.; Lin, Y.-Q. Thermochemical Characterization of Biochar from Cocoa Pod Husk Prepared at Low Pyrolysis Temperature. *Biomass Convers. Biorefinery* **2018**, *8*, 237–243. [CrossRef]
14. Tsai, W.-T.; Hsu, C.-H.; Lin, Y.-Q.; Tsai, C.-H.; Chen, W.-S.; Chang, Y.-T. Enhancing the Pore Properties and Adsorption Performance of Cocoa Pod Husk (CPH)-Derived Biochars via Post-Acid Treatment. *Process* **2020**, *8*, 144. [CrossRef]
15. Bahrun, A.; Yunus Fahimuddin, M.; Safuan, L.O.; Harjoni Kilowasid, L.M.; Singh, R. Effects of Cocoa Pod Husk Biochar on Growth of Cocoa Seedlings in Southeast Sulawesi-Indonesia. *Asian J. Crop Sci.* **2018**, *10*, 22–30. [CrossRef]
16. Ghysels, S.; Acosta, N.; Estrada, A.; Pala, M.; De Vrieze, J.; Ronsse, F.; Rabaey, K. Integrating Anaerobic Digestion and Slow Pyrolysis Improves the Product Portfolio of a Cocoa Waste Biorefinery. *Sustain. Energy Fuels* **2020**, *4*, 3712–3725. [CrossRef]
17. Rodriguez-Campos, J.; Escalona-Buendía, H.B.; Contreras-Ramos, S.M.; Orozco-Avila, I.; Jaramillo-Flores, E.; Lugo-Cervantes, E. Effect of Fermentation Time and Drying Temperature on Volatile Compounds in Cocoa. *Food Chem.* **2012**, *132*, 277–288. [CrossRef] [PubMed]
18. García, R.; Pizarro, C.; Lavín, A.G.; Bueno, J.L. Biomass Proximate Analysis Using Thermogravimetry. *Bioresour. Technol.* **2013**, *139*, 1–4. [CrossRef]
19. Carrier, M.; Loppinet-Serani, A.; Denux, D.; Lasnier, J.-M.; Ham-Pichavant, F.; Cansell, F.; Aymonier, C. Thermogravimetric Analysis as a New Method to Determine the Lignocellulosic Composition of Biomass. *Biomass Bioenergy* **2011**, *35*, 298–307. [CrossRef]
20. Grams, J. Chromatographic Analysis of Bio-Oil Formed in Fast Pyrolysis of Lignocellulosic Biomass. *Rev. Anal. Chem.* **2020**, *39*, 65–77. [CrossRef]
21. Lu, F.; Rodriguez-Garcia, J.; Van Damme, I.; Westwood, N.J.; Shaw, L.; Robinson, J.S.; Warren, G.; Chatzifragkou, A.; McQueen Mason, S.; Gomez, L.; et al. Valorisation Strategies for Cocoa Pod Husk and Its Fractions. *Curr. Opin. Green Sustain. Chem.* **2018**, *14*, 80–88. [CrossRef]
22. Rajkovich, S.; Enders, A.; Hanley, K.; Hyland, C.; Zimmerman, A.R.; Lehmann, J. Corn Growth and Nitrogen Nutrition after Additions of Biochars with Varying Properties to a Temperate Soil. *Biol. Fertil. Soils* **2012**, *48*, 271–284. [CrossRef]
23. Gaur, S.; Reed, T. *Thermal Data for Natural and Synthetic Fuels*; Taylor & Francis: New York, NY, USA, 1998; ISBN 9780824700706.
24. Manyà, J.J.; Velo, E.; Puigjaner, L. Kinetics of Biomass Pyrolysis: A Reformulated Three-Parallel-Reactions Model. *Ind. Eng. Chem. Res.* **2003**, *42*, 434–441. [CrossRef]
25. Domene, A.; Conesa, J. Biomasses Pyrolysis and Combustion Kinetics through N-Th Order Parallel Reactions. *Thermochim. Acta* **2011**, *523*, 176–181. [CrossRef]
26. White, J.E.; Catallo, W.J.; Legendre, B.L. Biomass Pyrolysis Kinetics: A Comparative Critical Review with Relevant Agricultural Residue Case Studies. *J. Anal. Appl. Pyrolysis* **2011**, *91*, 1–33. [CrossRef]
27. Kissinger, H.E. Reaction Kinetics in Differential Thermal Analysis. *Anal. Chem.* **1957**, *29*, 1702–1706. [CrossRef]
28. Chen, D.; Gao, X.; Dollimore, D. A Generalized Form of the Kissinger Equation. *Thermochim. Acta* **1993**, *215*, 109–117. [CrossRef]
29. García, A.N.; Marcilla, A.; Font, R. Thermogravimetric Kinetic Study of the Pyrolysis of Municipal Solid Waste. *Thermochim. Acta* **1995**, *254*, 277–304. [CrossRef]
30. Wang, L.; Lei, H.; Liu, J.; Bu, Q. Thermal Decomposition Behavior and Kinetics for Pyrolysis and Catalytic Pyrolysis of Douglas Fir. *RSC Adv.* **2018**, *8*, 2196–2202. [CrossRef]
31. Hameed, S.; Sharma, A.; Pareek, V.; Wu, H.; Yu, Y. A Review on Biomass Pyrolysis Models: Kinetic, Network and Mechanistic Models. *Biomass Bioenergy* **2019**, *123*, 104–122. [CrossRef]

32. Yang, H.; Yan, R.; Chen, H.; Lee, D.H.; Zheng, C. Characteristics of Hemicellulose, Cellulose and Lignin Pyrolysis. *Fuel* **2007**, *86*, 1781–1788. [CrossRef]
33. Zhou, X.; Li, W.; Mabon, R.; Broadbelt, L.J. A Critical Review on Hemicellulose Pyrolysis. *Energy Technol.* **2017**, *5*, 52–79. [CrossRef]
34. Kleinert, M.; Barth, T. Phenols from Lignin. *Chem. Eng. Technol.* **2008**, *31*, 736–745. [CrossRef]
35. Chen, L.; Liao, Y.; Guo, Z.; Cao, Y.; Ma, X. Products Distribution and Generation Pathway of Cellulose Pyrolysis. *J. Clean. Prod.* **2019**, *232*, 1309–1320. [CrossRef]